Javanmardi, Y. *et al*. *Géotechnique* [http://dx.doi.org/10.1680/jgeot.16.P.136]

A reference state curve to define the state of soils over a wide range of pressures and densities

Y. JAVANMARDI*, S. M. R. IMAM*, M. PASTOR† and D. MANZANAL†

Granular materials exhibit a behaviour that is strongly dependent on density, effective confining pressure and grain characteristics. The complexity is such that, in the past, for a given sand, loose and dense specimens, or specimens subjected to very low or very high confining pressures were considered as different materials and were modelled as such, using different constitutive parameters. The introduction of the state parameter improved both understanding of the behaviour and modelling of granular materials. Several alternative definitions have been proposed for the state parameter but they suffer from some limitations, especially when sand is very loose, has fines, or is subjected to high confining pressures. The purpose of this paper is to describe those deficiencies and to introduce a new state index based on a novel reference state curve. The proposed reference state curve is then applied to understanding and predicting some important aspects of soil behaviour such as: (*a*) stress ratios at the peak point of undrained effective stress paths and (*b*) the 'reverse behaviour' of sandy soils that show an unusual behaviour in undrained shearing under high effective confining pressure.

KEYWORDS: constitutive relations; particle crushing; soils

INTRODUCTION

The critical state line (CSL) is the fundamental component and the isotropic compression line (ICL) is an essential component of critical state soil mechanics (CSSM). For sands, slopes of both of these lines increase at high pressures in the plane of void ratio, e, against the logarithm of mean effective stress, p, and this increase has been attributed to breakage of sand particles (see e.g. De Souza, 1958; Coop & Lee, 1993; Vilhar *et al.*, 2013). Pestana & Whittle (1995) showed that, at sufficiently high stresses, different ICLs of a certain sand turn towards a near unique curve in the ln e–ln p plane, regardless of initial density. They called this line the limiting compression curve (LCC) (Fig. 1). Vesic & Clough (1968) showed that, when a wide range of stresses is considered, the CSL of sand consists of three segments, as shown in Fig. 1: a very-low-stress segment, an elevated-stress segment and a very-high-stress segment. At the elevated stress level, the LCC and CSL may become parallel (Muir Wood, 1990; McDowell *et al.*, 1996; Coop *et al.*, 2004) (Fig. 1).

Indices to describe soil state

Several indices have been proposed by researchers in order to understand, describe and normalise the behaviour of soils. These indices can be used either in advanced constitutive models (see e.g. Muir Wood *et al.*, 1994; Manzari & Dafalias, 1997; Li & Dafalias, 2000; Taiebat & Dafalias, 2008) or in simple formulas proposed for assessing typical behaviour of soils at various conditions.

Based on results of several triaxial tests on sand, Been & Jefferies (1985) defined the state parameter (ψ) as the vertical distance from the current state to the CSL in the e–ln p plane. However, several alternatives have also been proposed to define a state index for sandy soils (see e.g. Bauer, 1996; Wan & Guo, 1998; Wang *et al.*, 2002). For instance, Ishihara (1993) pointed out that application of ψ is less tenable in describing the behaviour of loose sands and Ishihara *et al.* (1998) introduced a new state parameter based on the loosest state of sands. Bobei *et al.* (2009) showed that ψ is unable to fully describe the behaviour of a mixture of sand with low percentage of fines and proposed a new state index to take into account effects of the added fines.

In order to take into account the effects of particle crushing, Russell & Khalili (2004) proposed a new reference curve to calculate a state index, which always takes negative values. Muir Wood & Maeda (2008) combined the CSL in the v–$\log p$ plane with a breakage index as the third axis, and presented a critical state surface (CSS) in the three-dimensional space, in which $v = 1 + e$ is the specific volume. Projection of the CSS onto the usual v–$\log p$ plane may be considered to consist of parallel lines, each corresponding to a specific breakage index (Fig. 2).

Several indices have been proposed to quantify the degree of particle breakage (see e.g. Marsal, 1967; Miura & O-Hara, 1979; Hardin, 1985; Muir Wood, 2007). In the current study, the breakage index (B_{10}) proposed by Lade *et al.* (1996) is used owing to the possibility of its determination using commonly available test data. This index is defined as

$$B_{10} = 1 - \frac{D_{10f}}{D_{10i}} \tag{1}$$

in which D_{10f} and D_{10i} are the effective grain sizes of the final and initial gradations, respectively. Effective grain size is the maximum particle size of the smallest 10% of the aggregate. Owing to the difficulty of determination of evolving gradations during tests, Lade *et al.* (1996) suggested the following hyperbolic equation to estimate B_{10}

$$B_{10} = \frac{E_T}{a + E_T} \tag{2a}$$

$$E_T = \int p\,\dot{\varepsilon}_v + \int q\,\dot{\varepsilon}_q \tag{2b}$$

Manuscript received 6 June 2016; revised manuscript accepted 13 April 2017.
Discussion on this paper is welcomed by the editor.
* Department of Civil and Environmental Engineering, Amirkabir University of Technology, Tehran, Iran.
† M^2i (Mathematics Modelling Engineering) Group, Department of Applied Mathematics, Escuela Técnica Superior de Ingenieros de Caminos, Universitad Politécnica de Madrid, Madrid, Spain; INTECIN, CONICET, Buenos Aires, Argentina.

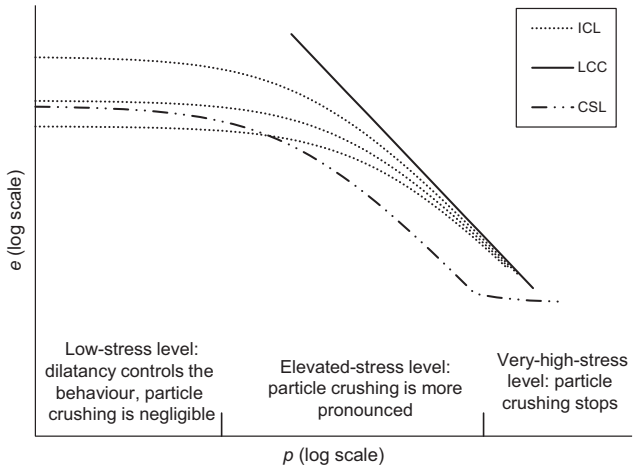

Fig. 1. Schematic representation of three ICLs, full stress range CSL and LCC of a sand

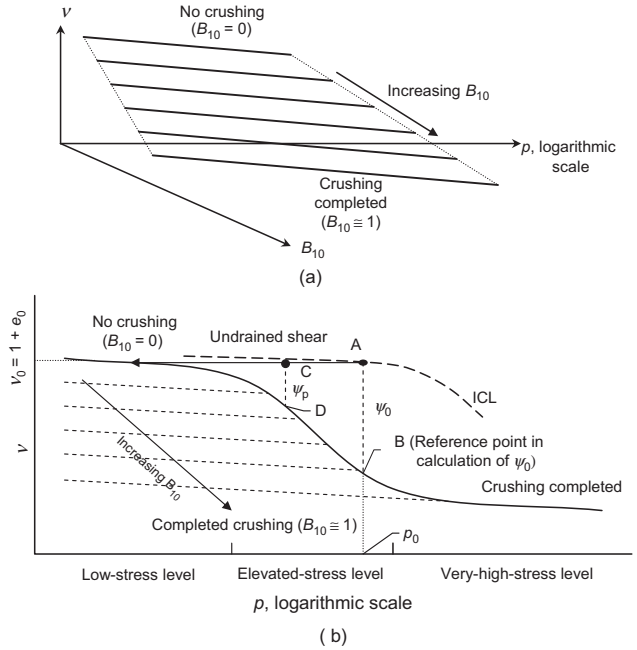

Fig. 2. (a) Critical state surface in three-dimensional space and change in breakage index; (b) projection of critical state surface in specific volume–logarithm of mean effective stress plane

in which a is a material constant (in MPa), which was determined to be 0·747 MPa for Cambria sand (Lade *et al.*, 1996). E_T is the total energy input per unit volume of specimen (MPa), which is determined by calculating the area under stress–strain (p–ε_v and q–ε_q) curves during both consolidation and shearing. q is deviatoric stress. ε_v and ε_q are volumetric and deviatoric strains, respectively. The overdot indicates an increment.

For clays, the overconsolidation ratio (OCR) is usually used to normalise the behaviour (Ladd & Foott, 1974), and the normal consolidation line (NCL) rather than the CSL is used as the reference line. Indeed, different approaches are adopted to define the state index for clays and sands. This may raise questions about the definition of a proper state index for a mixture of sand and clay, which may exhibit an intermediate behaviour.

Although the state parameter proposed by Been & Jefferies (1985) allows a better understanding of the behaviour of granular soils at various densities and effective confining pressures, it has some deficiencies, especially at high confining pressures, high void ratios and when fines are present. The following section describes some of these deficiencies; also, a new state index will later be introduced which is based on a novel reference state curve (RSC). It will be shown that the variation of the stress ratio at peak point of the undrained effective stress path (UESP) of soils can be correlated to this index over a wide range of confining pressures and void ratios. The so-called reverse behaviour of some sandy soils can also be described readily using such a reference curve. Furthermore, this index can be used in normalising the behaviour of both sands and clays.

SOME DEFICIENCIES OF Ψ

Figure 2(b) shows the initial state parameter, ψ_0, of a sand specimen consolidated to void ratio e_0 and confining pressure p_0 (point A). The ICL that passes through A is also depicted in the figure. Since the slope of the ICL has not changed yet at point A, the amount of particle breakage due to consolidation up to point A is negligible and $B_{10} \cong 0$. If the specimen is then sheared in undrained loading, its state will move to the left and eventually reaches the very-low-stress segment of the CSL. Thus, at the end of shearing, the particle breakage is insignificant and the initial and final gradation curves of the sample are similar. However, the reference point used to calculate ψ_0 (point B) is located on the elevated-stress segment of the CSL, which corresponds to a non-zero value of B_{10}. In other words, point B corresponds to a soil with different gradation and, in calculating ψ_0, the state of soil at A is compared with the state of another soil at point B. Therefore, point B does not seem to be an appropriate reference point to define a state index for this sample and ψ_0 is not a suitable index to describe its behaviour (Ghafghazi *et al.*, 2014). In order to properly define a state index, it is more reasonable to choose a reference line that corresponds to the same amount of particle breakage at both the current and reference states (Muir Wood & Maeda, 2008). Nevertheless, if the sample is consolidated at lower pressures such that the location of point A remains on the very-low-stress zone of the CSL, the gradation curves at point A and at the reference point on the CSL are expected to be similar. Therefore, for such samples ψ_0 would be a suitable state parameter to describe the soil behaviour.

Loose and very loose sands typically exhibit a peak in their UESP. The stress states at the peak point of the UESP (P-UESP) of such sands have been identified by defining various lines and surfaces, such as the critical stress ratio line (Vaid & Chern, 1985), the collapse surface (Sladen *et al.*, 1985) and the instability line (Lade, 1992). Determination of this stress state is of significant importance in some geotechnical applications since loss of shear strength in undrained loading initiates at this stress state.

The P-UESP usually occurs at relatively small strains. As a result, total (or plastic) energy input per unit volume of the specimen and, consequently, the degree of particle breakage due to shearing are relatively small before this point is reached. This is shown in Fig. 3, which represents the undrained stress–strain curve and stress path of a sample of Cambria sand. Using equation (2), B_{10} is calculated at several points of the stress–strain curve and depicted next to the corresponding data points. During the consolidation stage, particle breakage takes place, and B_{10} increases until it finally reaches the value of 0·41. During the shearing stage, B_{10} does not change significantly before the stress path reaches the P-UESP, but it starts taking larger values after that.

Figure 4 shows the correlation between M_p and $\sin\phi_p$ with ψ_0 for triaxial compression (TC) tests on Toyoura sand, in which $M = q/p$ is the stress ratio with $q = \sigma_1 - \sigma_3$, $p = (\sigma_1 + 2\sigma_3)/3$, σ_1 and σ_3 are the major and minor principal

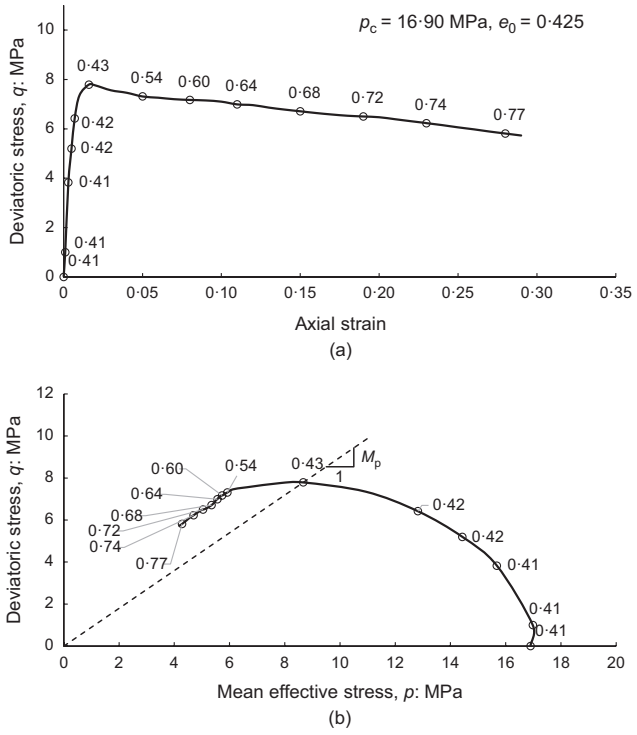

Fig. 3. (a) Deviatoric stress–axial strain curve; (b) stress path obtained from a sample of Cambria sand in triaxial undrained test. B_{10} is depicted beside each data point (test data from Bopp & Lade (2005))

stresses, respectively, and M_p and ϕ_p are the stress ratio and mobilised friction angle at P-UESP, respectively. The consolidation pressures of the samples are depicted beside the data points. Based on data from hollow cylinder tests, Imam *et al*. (2002a) showed that a similar linear relationship exists between M_p and $\sin\phi_p$ with ψ. However, compared to stress ratio, the slope of variation of $\sin\phi_p$ with ψ is less affected by the direction of loading (anisotropy) and the intermediate principal stress; therefore, $\sin\phi_p$ is a more suitable variable for use in constitutive modelling.

Figure 4 shows that a linear relationship exists between M_p (or $\sin\phi_p$) and ψ_0 for specimens consolidated at pressures lower than 1000 kPa, as depicted by the dashed line in this figure. At a confining pressure of about 1000 kPa, the slope of CSL of Toyoura sand increases. Meanwhile, points corresponding to specimens consolidated at pressures equal or higher than this value do not lie on the dashed line, and their distance from the dashed line increases with the increase in confining pressure. In other words, $\sin\phi_p$ cannot be well correlated with ψ_0 over a wide range of consolidation pressures. This deficiency may be considered as a practical consequence of the first deficiency discussed before. This means that the initial states of the samples consolidated at pressures less than 1000 kPa are located at the low stress zone of the CSL. Therefore, in such regions, ψ_0 is an appropriate parameter to normalise the behaviour, and a linear relationship exists between $\sin\phi_p$ and ψ_0. However, when the consolidation pressure exceeds approximately 1000 kPa, the initial states of the samples will be located on the elevated-stress segment of the CSL and, as noted before, ψ_0 is unable to describe the behaviour well or be correlated with $\sin\phi_p$.

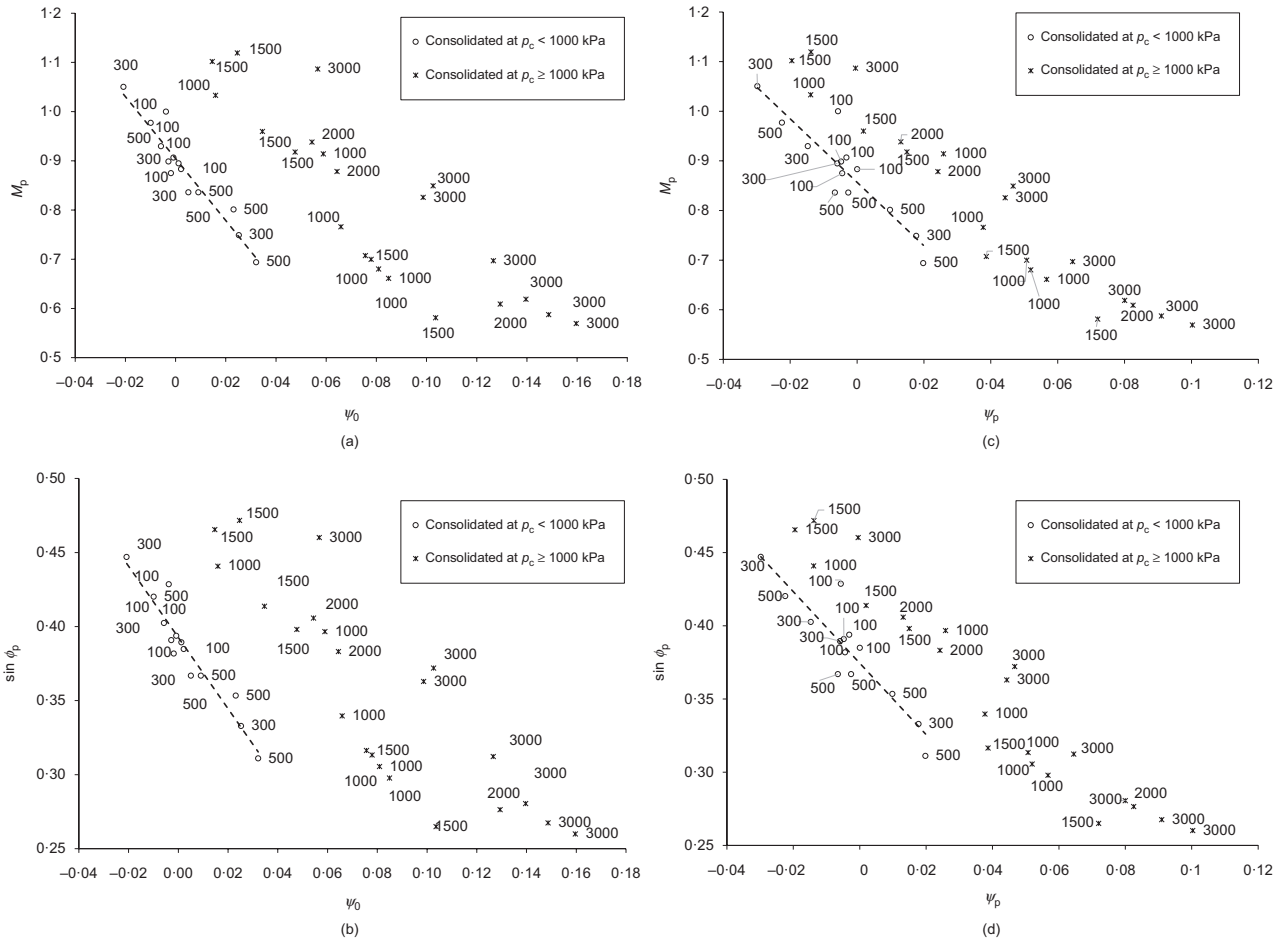

Fig. 4. Relationship between (a) M_p and ψ_0, (b) $\sin\phi_p$ and ψ_0, (c) M_p and ψ_p, and (d) $\sin\phi_p$ and ψ_p for Toyoura sand. Confining pressures are depicted next to each data point (test data from Verdugo (1992))

In Figs 4(c) and 4(d), ψ_0 has been replaced with the current state parameter at P-UESP, ψ_p. These figures show that a proper correlation is not obtained between $\sin\phi_p$ (or M_p) and ψ_p either. This can be explained readily using Fig. 2(b). Ishihara (1993) showed that the P-UESP occurs at a mean effective stress approximately 0·61 times the confining pressure (point C in Fig. 2(b)). Since, during shearing, the degree of particle breakage before P-UEST is negligible (see Fig. 3), B_{10} takes similar values at points A and C. However, the reference point used to calculate ψ_p (point D in Fig. 2(b)) is located on the elevated-stress segment of the CSL. Therefore, the grading of soil and magnitude of B_{10} would be different at points C and D, and ψ_p will have the same deficiency as ψ_0 in its correlation with M_p or $\sin\phi_p$ as described before.

Lade & Yamamuro (1997) and Yamamuro & Lade (1998) investigated the undrained behaviour of a mixture of sand with a low percentage of fines. They showed that, unlike clean sand, increasing the confining pressure for samples consolidated on certain ICLs decreases their contractive response and liquefaction potential in undrained shearing. They referred to such behaviour as the 'reverse behaviour'. Reverse behaviour has also been observed by several other researchers (see e.g. Bobei *et al*., 2009; Rahman & Lo, 2014) in sand with fines.

In order to describe the reverse behaviour more clearly, first the normal behaviour usually observed in clean sands will be considered. Fig. 5(a) illustrates an ICL and the CSL of Toyoura sand. The initial states of three specimens consolidated to points A, B and C on the ICL, and values of void ratio, confining pressure and ψ_0 at consolidation are also shown in Fig. 5(a). Fig. 5(b) shows the normalised stress–strain response of these samples under TC tests and indicates that samples consolidated to higher confining pressures exhibit more contractive behaviour and liquefaction potential (less stable behaviour) as expected and, therefore, this is referred to as normal behaviour. This is also consistent with the definition of ψ_0 such that an increase in its value is associated with a more contractive and less stable behaviour. Therefore, the occurrence of normal behaviour can be predicted using the initial state parameter.

The CSL and an ICL of Sydney sand mixed with 10% fines are plotted in Fig. 6(a). The initial states of specimens A, B and C consolidated to confining pressures of 100 kPa, 400 kPa and 1115 kPa, respectively, are also shown in the figure. Values of ψ_0 are 0·049, 0·0495 and 0·050 for these samples, respectively. The value of ψ_0 is slightly smaller for specimen A but, as shown in Fig. 6(b), it fully liquefied whereas specimens B and C exhibited more stable behaviours. Samples B and C have approximately the same (or slightly higher) values of ψ_0. Therefore, it is expected that such samples exhibit similar (or slightly more contractive) behaviour. However, less contractive behaviour and liquefaction potential are observed for these specimens. This kind of behaviour is regarded as the reverse behaviour. Based on such experimental results, Bobei *et al*. (2009) concluded that ψ_0 does not seem to be able to take into account the reverse behaviour of sands with fines.

EQUATIONS USED FOR THE ICL, LCC AND CSL

Butterfield (1979) proposed the compression curve in double logarithmic $\ln v$–$\ln p$ plane and Pestana & Whittle (1995) proposed a linear relationship for the LCC of soils in the $\ln e$–$\ln p$ plane that can be written in the following form

$$\ln e = \ln N - \lambda \ln p \tag{3}$$

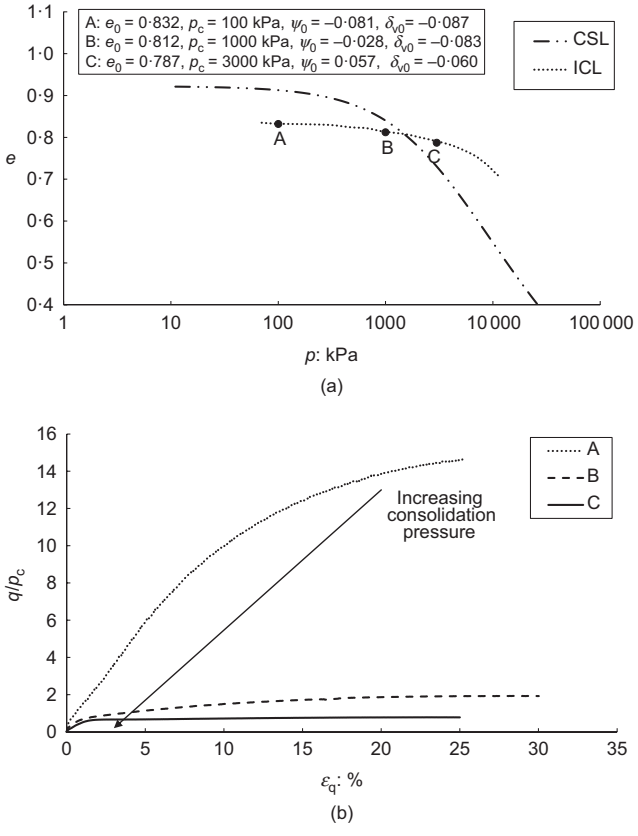

Fig. 5. Effect of consolidation pressure on liquefaction potential of Toyoura sand in undrained test: (a) initial state of three samples; (b) normalised stress–strain response of the samples (test data from Verdugo (1992))

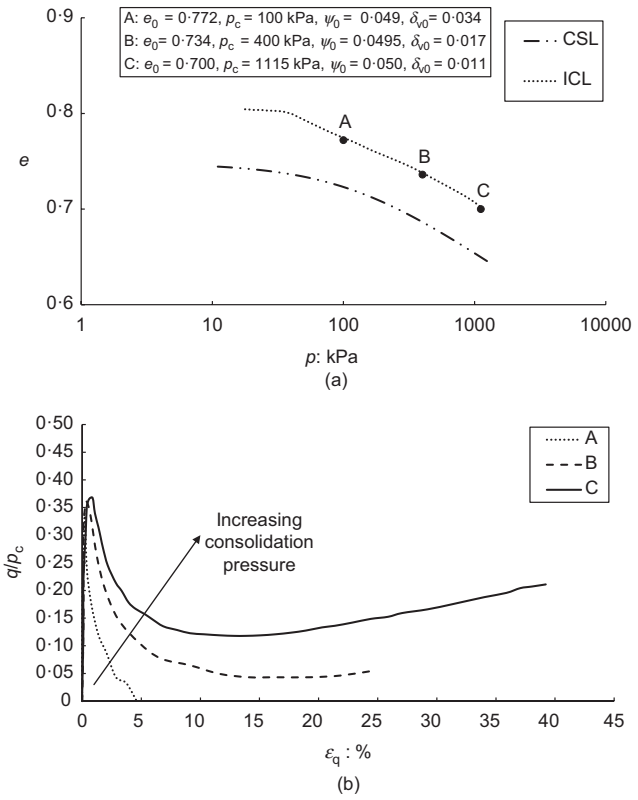

Fig. 6. Effect of consolidation pressure on liquefaction potential of Sydney sand with 10% fines in undrained tests: (a) initial states; (b) normalised stress–strain responses (test data from Bobei *et al.* (2009))

in which λ is the slope of the LCC in the double logarithmic space and N is the void ratio on the LCC at $p = 1$ (unit stress). The NCL of clays is usually plotted in the e–log p plane. However, Pestana & Whittle (1999) used equation (3) for such materials and presented it in the ln e–ln p space.

Sheng *et al*. (2008) suggested the following equations to approximate the ICL and the CSL of sands

$$\text{ICL}: \quad \ln e = \ln N - \lambda \ln (p + p_r) \tag{4}$$

$$\text{CSL}: \quad \ln e = \ln \Gamma - \lambda \ln (p + p_{cr}) \tag{5}$$

in which p_r and p_{cr} control the curvature of the ICL and the CSL, respectively. p_{cr} is a material parameter and, for a certain ICL, p_r is constant and dependent on the initial void ratio of the ICL. Γ is the void ratio at $p + p_{cr} = 1$ (unit stress) on the CSL and λ is the slope of the asymptote line to the CSL at the elevated stress level, which is assumed to be identical to the slope of LCC.

The CSL and ICL of three sandy soils and one clayey soil are shown in Fig. 7 using equations (4) and (5), respectively. Experimental data and physical properties of the soils are adopted from the references provided in Table 1.

As can be noticed from Fig. 7, the ICL and CSL of both the sandy soils and the clayey soil can be modelled well using equations (4) and (5). Therefore, these equations are used to simulate the ICL and the CSL in the current study.

PROPOSED REFERENCE CURVE AND STATE INDEX

Before introducing the new reference state curve, the CSS will be examined more closely. The aim is to calculate the initial state index at several states located on an ICL using the CSS as the reference surface. Based on Fig. 2(b), the projection of the CSS onto the two-dimensional plane consists of parallel lines, each corresponding to a certain B_{10}. Here, these lines are referred to as iso-breakage lines. For each state, the state index should be calculated with respect to an iso-breakage line with the same value of B_{10}.

Figure 8 shows the CSL and ICL of Cambria sand up to very high confining pressures. B_{10} was calculated at several data points on these lines using equation (2) and was displayed beside each point. Point B in Fig. 8 represents the state of a specimen that has been isotropically consolidated up to very high pressures, so that $(B_{10})_B \cong 1$. In order to calculate the proper state index at this point, the iso-breakage line which corresponds to $B_{10} \cong 1$ must be found.

Point A in Fig. 8 is located on the CSL and the gradation curve of the soil at this point has reached a limiting condition at which $(B_{10})_A \cong 1$. Therefore, the iso-breakage line that corresponds to $B_{10} \cong 1$ must pass through point A, and should be parallel to the CSL at the low-stress segment. This is the lowest dashed line shown in Fig. 8.

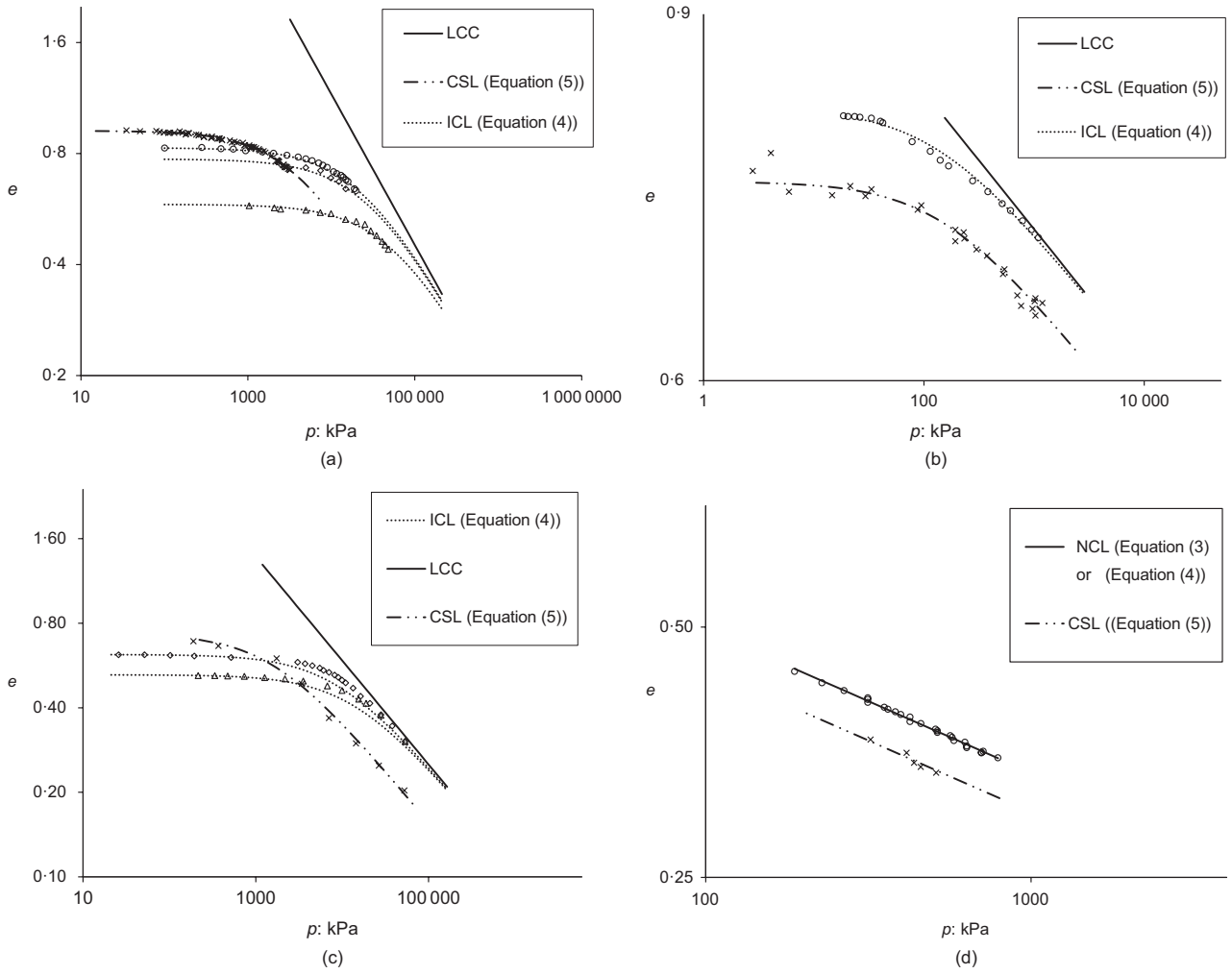

Fig. 7. Comparison of ICL and CSL in double logarithmic void ratio–mean effective stress space with test results for several soils (test data from references shown in Table 1): (a) Toyoura sand, $p_{cr} = 3900$ kPa, $\lambda = 0{\cdot}409$, $\Gamma = 27{\cdot}14$, $N = 44{\cdot}33$; (b) Cambria sand, $p_{cr} = 1550$ kPa, $\lambda = 0{\cdot}370$, $\Gamma = 11{\cdot}12$, $N = 17{\cdot}79$; (c) Sydney 2 sand, $p_{cr} = 150$ kPa, $\lambda = 0{\cdot}066$, $\Gamma = 1{\cdot}041$, $N = 1{\cdot}12$; (d) Lower Cromer Till, $p_{cr} = 0$, $\lambda = 0{\cdot}172$, $\Gamma = 0{\cdot}98$, $N = 1{\cdot}096$, $p_r = 0$

Table 1. Physical properties of soils

	Specific gravity G_s	Fines content, FC: %	Mean diameter, D_{50}: mm	Max. void ratio, e_{max}	Min. void ratio, e_{min}	Mineralogy of the host soil	Reference
Toyoura	2·65	0	0·17	0·977	0·597	Quartz, feldspar, magnetite	Verdugo (1992) – Miura *et al.* (1984)
Sydney	2·61	10					Bobei *et al.* (2009)
Cambria	2·69	0	1·66	0·792	0·503	Quartz, sedimentary, metamorphic and volcanic lithic grain	Bopp & Lade (2005)
Lower Cromer Till		17% clay				Calcite, Illite	Pestana (1994)

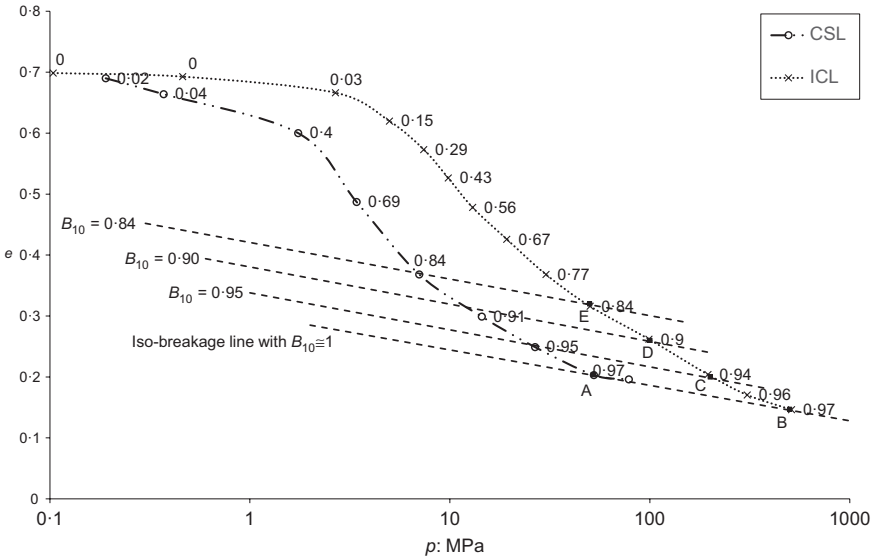

Fig. 8. Particle breakage indices (B_{10}) at ICL and CSL for Cambria sand with iso-breakage reference lines for $B_{10} = 1$, 0·95, 0·9 and 0·84 (test data from Lade *et al.* (1996))

Points C, D and E in Fig. 8 represent the state of samples at consolidation for $B_{10} = 0{\cdot}95$, 0·90 and 0·84, respectively. The corresponding iso-breakage lines are also depicted in the figure. As can be noticed, the vertical distances from points B, C, D and E to the corresponding iso-breakage lines are approximately zero. All these points are located in the region where the CSL and LCC are parallel in ln e–ln p space (see Fig. 7(b)). Therefore, at such region, a proper initial state index takes values close to zero.

In the above approach, different iso-breakage lines were used to calculate the state index. Now, the purpose is to replace such different reference lines with a single reference curve. Based on the above discussions, such a unique curve should have two features: (*a*) since the proper value of the initial state index at high stresses is close to zero, this curve should be close to the LCC at such pressures; (*b*) since the CSL is a suitable reference line to define soil states in the low-stress region, this curve should be parallel or close to the CSL at low confining pressures.

Since the CSL and the LCC are parallel at the elevated stress segment, if the CSL is shifted horizontally such that its elevated stress segment approaches the LCC asymptotically, a new curve is obtained. This curve, which is referred to as the RSC here, can satisfy both features mentioned above. The RSC, which is illustrated schematically in Fig. 9, is defined in the usual two-dimensional space and no additional axis is required to take into account the effects of particle breakage.

As, for a given soil, the CSL and LCC are unique and independent of the initial soil state, it is expected that the RSC would also be unique and independent of the initial void ratio, mean effective stress and fabric of the specimens.

Assuming that the LCC and CSL can be determined by equations (3) and (5), the equation for the RSC can be obtained as follows

$$\text{RSC}: \quad \ln e = \ln \Gamma - \lambda \ln\left[\frac{p}{\exp(\Delta)} + p_{cr}\right] \tag{6}$$

in which Δ is a dimensionless parameter which provides the horizontal distance between the CSL and the LCC in the ln e–ln p plane, as shown in Fig. 9(a). The vertical distances from the RSC can be used to define a state index, as shown in Fig. 9(b).

It is possible to define the RSC for clays, as well as granular materials. Since the CSL and NCL of clays are assumed to be linear and parallel to each other in the ln e–ln p space, the RSC will coincide with the NCL of clays. The initial state index is given by the vertical distance from the initial state to the NCL (or the RSC) and this distance is proportional to ln (OCR). Therefore, the new state index can play a role similar to that of the OCR for clays.

A SIMPLE METHOD TO APPROXIMATE THE RSC

The CSL and RSC of Toyoura sand are illustrated in Fig. 10. Point A is located on the CSL at very low stress, namely, $p_A \cong 0$. The ICL that passes through point A will be referred to as the ICL-A, and is simulated by equation (4) and shown in this figure. As point A is located on both the

CSL and the ICL-A and $p_A \cong 0$, the following relationships can be written

$$\ln e_A = \ln \Gamma - \lambda \ln p_{cr} \tag{7a}$$

$$\ln e_A = \ln N - \lambda \ln (p_r)_A \tag{7b}$$

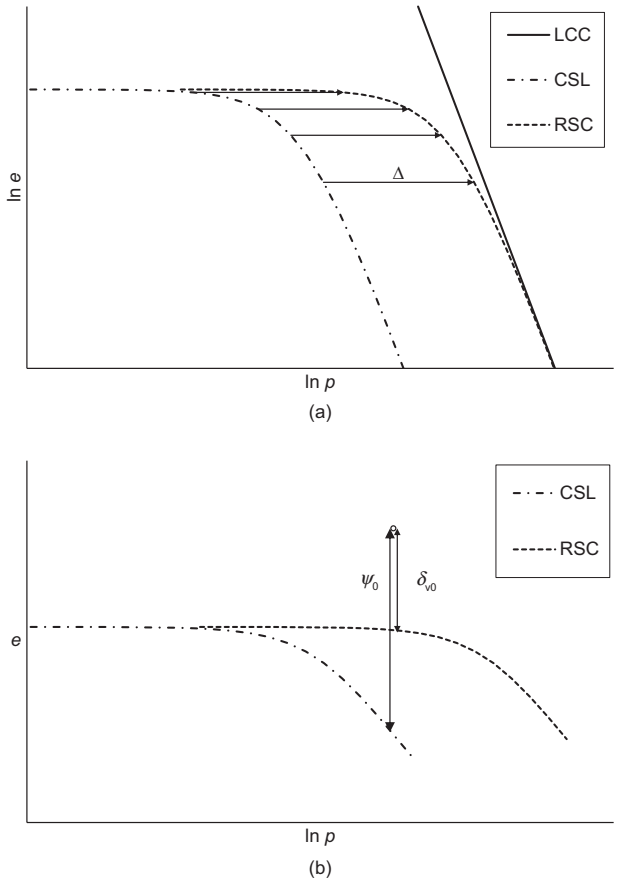

Fig. 9. (a) Schematic representation of CSL, LCC and RSC in the ln *e*–ln *p* space; (b) initial state parameter (ψ_0) and initial state index (δ_{v0})

where e_A is the void ratio at point A. Using equations (3) and (5) and the definition of Δ, it is possible to obtain $N = \Gamma \exp(\lambda\Delta)$. Therefore, $(p_r)_A = p_{cr}\exp(\Delta)$, from which the equation for the ICL-A is obtained as

$$\ln e = \ln \Gamma - \lambda \ln\left(\frac{p}{\exp \Delta} + p_{cr}\right) \tag{8}$$

This equation is identical to equation (6) describing the RSC. Consequently, ICL-A coincides with the RSC. This result is applicable to all sands and provides a simple method to approximate the RSC. Therefore, in order to obtain the RSC it would be sufficient to find a point on the CSL at a very low stress and conduct an isotropic consolidation test on a specimen at such initial state. The resulting ICL will be a good approximation of the RSC. In other words, it might be concluded that the RSC is an isotropic compression curve in nature, similar to the NCL, which is used as the reference curve to calculate the OCR for clays. Furthermore, the RSC can be determined by a single isotropic compression test and is independent of the CSL and the value of Δ. Hence, equation (6) for the RSC can be rewritten in the following form

$$\ln e = \ln N - \lambda \ln (p + p'_r) \tag{9}$$

in which, $p'_r = p_{cr}\exp(\Delta)$ is a material constant describing the curvature of the RSC.

Figure 10 shows the CSL, RSC and two ICLs of Toyoura sand. As noted before, there exists a correlation between the amount of particle breakage and the magnitude of total work input to the specimen. Therefore, the total energy has been calculated at several points on the ICLs and CSL and is depicted beside each data point in Fig. 10 as an indication of the degree of particle breakage. The material parameter a is not available for Toyoura sand, hence B_{10} could not be calculated for this soil. As can be noticed from Fig. 10, at a given mean effective stress, the difference between total energy of samples located on each of the ICLs and the CSL is significant, whereas if the RSC (or ICL-A) is used as the reference line instead of the CSL, this difference will decrease substantially. Therefore, the amount of particle breakage at the RSC is more similar to the amount of particle breakage at the initial state of samples.

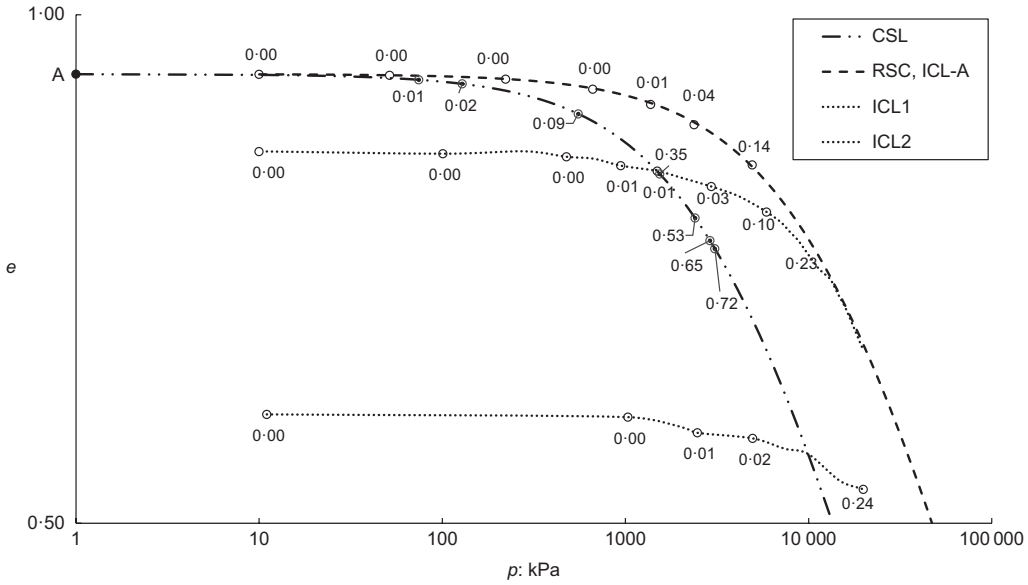

Fig. 10. Relationship between the RSC and the ICL-A of Toyoura sand, total energy input per unit volume is depicted next to each data point (test data from Verdugo (1992))

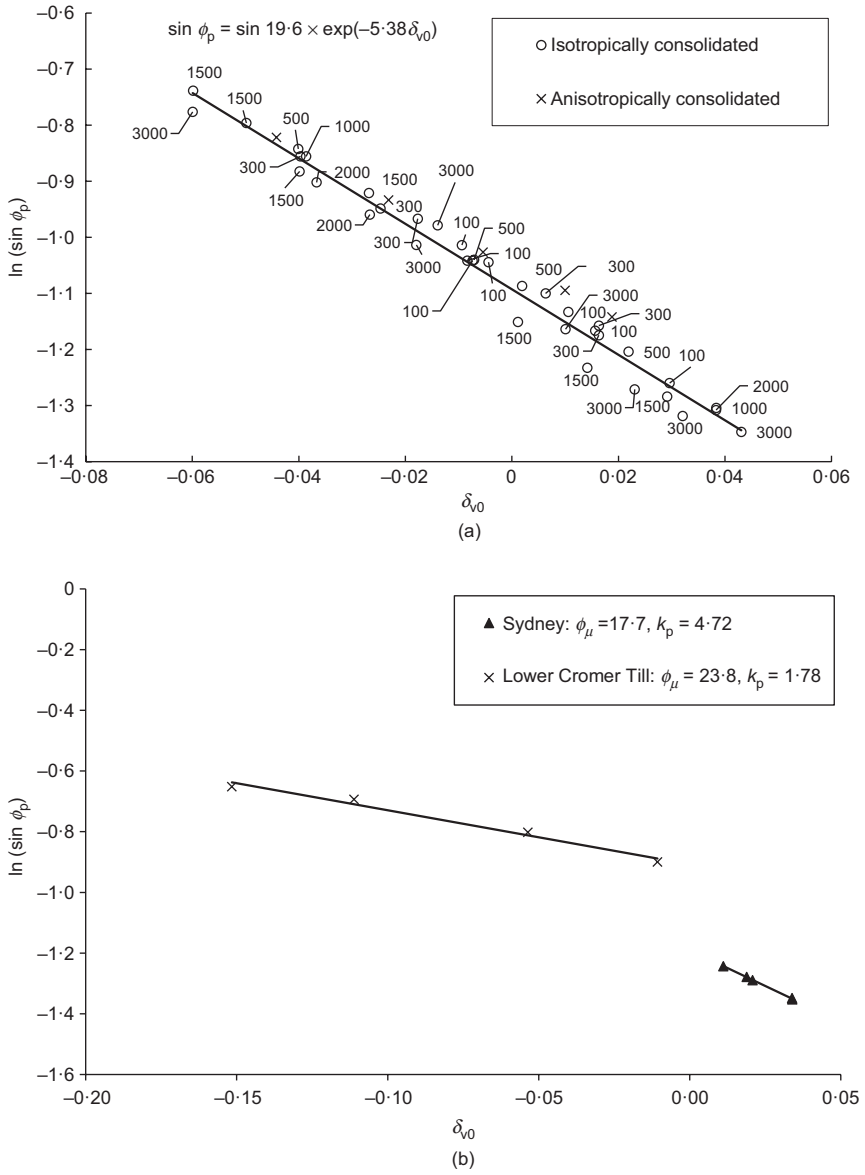

Fig. 11. Determination of ϕ_μ and k_p for (a) Toyoura sand and (b) Sydney sand with 10% fines, and Lower Cromer Till (mixture of clay and granular materials) (data references in Table 1)

SOME APPLICATIONS OF THE RSC

Correlations with the friction angle at the P-UESP

In order to estimate the friction angle at P-UESP, $\sin\phi_p$, the difference in void ratio between the initial state and the RSC will be used to define the state index as follows

$$\delta_{v0} = e_0 - e_{RSC} \tag{10}$$

in which e_0 is the initial void ratio and e_{RSC} is the void ratio at a point on the RSC with the same mean effective stress. Fig. 11 shows that the relationship between $\ln(\sin\phi_p)$ and δ_{v0} is linear for three soils, even when a wide range of consolidation pressures are considered. Therefore, to estimate the mobilised friction angle at P-UESP (ϕ_p), the following exponential relationship can be used

$$\sin\phi_p = A\exp(-k_p\delta_{v0}) \tag{11}$$

in which k_p and A are material constants. To determine these parameters, a series of undrained TC tests exhibiting a peak in their UESP is required. The magnitude of A is typically close to $\sin\phi_\mu$, in which ϕ_μ is the inter-particle friction angle. Thus, equation (11) can be rewritten in the following form

$$\sin\phi_p = \sin\phi_\mu\exp(-k_p\delta_{v0}) \tag{12}$$

Figure 11(a) illustrates data from both isotropically and anisotropically consolidated tests on Toyoura sand and the numbers beside each data point indicate the consolidation pressure. Fig. 11(b) shows that equation (12) is also applicable to Sydney sand mixed with 10% fines. Data for the Lower Cromer Till (LCT), which is a mixture of clay and granular materials, are also shown in Fig. 11. The material constants used to describe the CSL, LCC, RSC and the inter-particle friction angle are presented in Table 2 for these soils.

The effect of using δ_{v0} on improving the correlations may be noticed by comparing Figs 4(b) and 11(a). This comparison indicates that the positions of the specimens consolidated at pressures less than 1000 kPa are nearly the same in both figures. This is because at low stresses, the RSC of Toyoura sand is close to the CSL and ψ_0 and δ_{v0} are therefore approximately equal. However, at the elevated-stress zone, the RSC is located above the CSL (see Fig. 10) and δ_{v0} is smaller than ψ_0 (see Fig. 9(b)), and changing the abscissa of Fig. 4(b) from ψ_0 to δ_{v0} shifts the points corresponding to such samples to the left horizontally. The distance between the RSC and CSL and, consequently, the magnitude

Table 2. Material parameters used for the data shown in Fig. 7 and Fig. 11

	p_{cr}: kPa	λ	Γ	Δ	ϕ_μ	k_p	ϕ_{cs}
Toyoura sand	3900	0·409	27·14	1·2	19·6	5·38	31·4
Cambria sand	1550	0·37	11·12	1·27	20	—	36·1
Sydney sand	150	0·066	1·041	1·1	17·7	4·72	35·0
Lower Cromer Till	0	0·172	0·98	0·65	23·8	1·78	30·0

of this shift increases at higher confining pressures. Therefore, a unique correlation is obtained in the δ_{v0}–ln(sin ϕ_p) plane regardless of the consolidation pressures.

In normally consolidated (NC) clays, the undrained effective stress path exhibits a peak strength near the CSL and, therefore, $\phi_p \cong \phi_{cs}$. The initial state of such soils is located on the NCL. Since the RSC coincides with the NCL, $\delta_{v0} = 0$ for NC samples and, according to equation (12), $\phi_\mu = \phi_p$. Inter-particle friction angle does not have a clear meaning for clays. Consequently, a value of ϕ_μ close to the friction angle at critical state may be used for such materials in equation (12). Table 2 shows that ϕ_μ is not equal to ϕ_{cs} for LCT, because this soil is not a pure clay, but the difference between these two friction angles is less than those for the sandy soils.

Furthermore, equation (12) may be used in the development of constitutive models for soils. In clays, the yield surface is often described by an ellipse with the stress ratio at its peak being equal to M_{cs} (see e.g. Roscoe & Burland, 1968). On the other hand, Imam *et al*. (2005) used M_p as the stress ratio at the peak of the yield surface of sands. Therefore, for both clays and sands, M_p, which may be estimated using equation (12), can be used to determine the stress ratio at the peak point of yield surfaces. This equation may therefore be useful in the development of unified constitutive models for sands, clays and mixed soils.

It is expected that samples with the same value of δ_{v0} exhibit similar values of sinϕ_p in undrained tests. In order to examine this, the CSL and RSC of Toyoura sand are shown in the e–ln p space in Fig. 12. Data points correspond to states at consolidation for several undrained TC tests. Values of sinϕ_p measured from those tests are also shown next to each data point. Using these data, contour lines corresponding to sin$\phi_p = 0{\cdot}28$, $0{\cdot}34$ and $0{\cdot}42$ are plotted. It may be noticed that contours of sinϕ_p are approximately parallel to the RSC. Points located on a certain contour line have the same δ_{v0} and exhibit the same value of sinϕ_p (or M_p), but correspond to different values of ψ_0. This indicates that δ_{v0} is better correlated to sinϕ_p than ψ_0.

In the application described above, the RSC was used as an alternative for the CSS to define the state index and estimate M_p. Two main factors may be considered to be combined in defining state indices using the CSS: (*a*) the degree of particle breakage and (*b*) the distance to the critical state, the latter being a measure of the amount of large inter-particle slip and grain rotation needed to change the soil volume and fabric in order to reach critical state. These changes, in turn, generate plastic strains. It seems, however, that in the case of the P-UESP, the first factor plays a more important role. Considering the relatively small strain that usually occurs when the P-UESP is reached (see Fig. 3), the effects of initial fabric are expected to still exist at this state. Imam *et al*. (2002a, 2002b) showed detailed evidence of this, and Yoshimine (1996) showed that the effects of fabric and specimen preparation are quite pronounced when the P-UESP is reached, while these effects decrease during shearing and are very small or eliminated when the phase transformation or the critical state is reached. This suggests that, before the P-UESP is reached, the mechanisms that

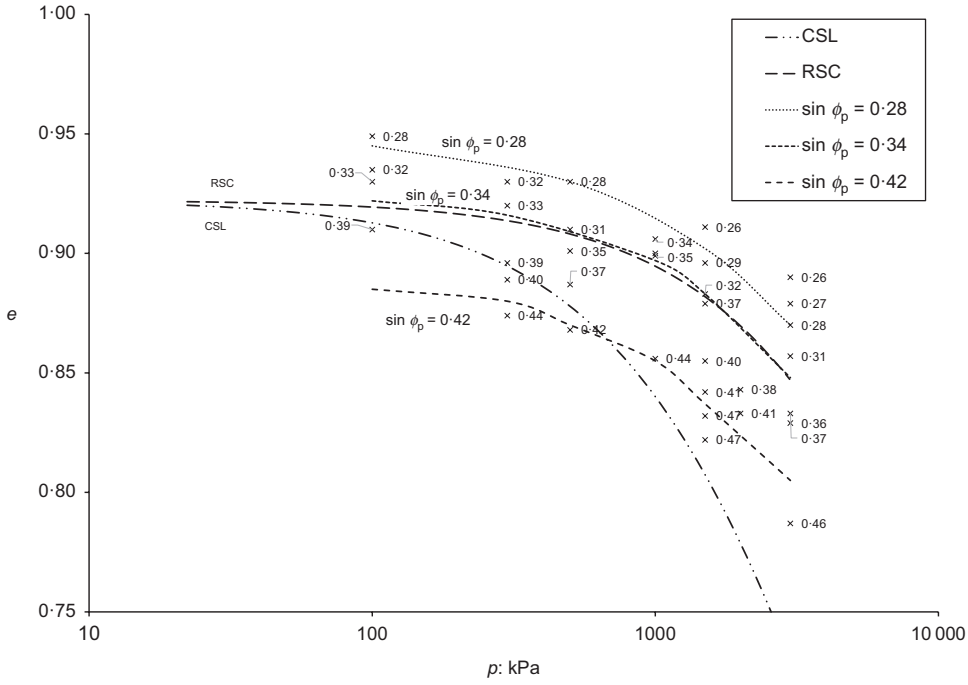

Fig. 12. Initial states of samples of Toyoura sand with values of sinϕ_p depicted beside each data point. Contours of sin $\phi_p = 0{\cdot}28$, $0{\cdot}34$, $0{\cdot}42$ are also shown (test data from Verdugo, (1992))

cause the movement of grains, the occurrence of large inter-particle slip or rotation, the change in the soil fabric and the large plastic strains that finally propel the fabric towards the ultimate state, have not been initiated yet. In conclusion, for P-UESP, although the second factor (distance to the ultimate state) may have some effects, it plays a less important role compared to the effects of the first factor (particle breakage). This may be the reason for the use of the inter-particle rather than the constant volume (critical state) friction angle in correlations proposed for the prediction of $\sin\phi_p$ (see e. g. Imam *et al*., 2002a, 2002b).

Prediction of the reverse behaviour

Results shown in Fig. 5 indicated that clean sand exhibits a normal, expected behaviour in which increasing confining pressure results in an increase in liquefaction potential. However, an unexpected, reverse behaviour is observed in Sydney sand with 10% fines, in that liquefaction potential decreases with the increase in confining pressures. Yamamuro & Lade (1998) attributed this reverse behaviour to initial fabric and compressibility of the soil mixture. Rahman & Lo (2014) pointed out that the position of the ICL is usually located above the CSL for sand with fines and this, also, affects the occurrence of reverse behaviour. In this sense, the reverse behaviour may not be a behaviour of only mixed sands, but it may also be observed in clean sand consolidated on an ICL above the RSC. This is presented in Fig. 13. This figure shows the initial states of three samples of Toyoura sand. Fig. 13(b) shows that samples consolidated at higher pressures show a more stable behaviour and less liquefaction potential.

The RSC is an ICL in nature, which coincides with the CSL at very low stresses. The effect of increasing confining pressure on the behaviour of samples consolidated on such ICL (i.e. RSC) is shown in Fig. 14. The value of δ_{v0} is close to zero for all three samples shown in this figure and Fig. 14(b) indicates that these samples exhibit rather similar normalised behaviours. In other words, samples consolidated to states on the RSC do not exhibit normal or reverse behaviours, but a neutral behaviour for which change in confining pressure would not affect their normalised response.

Figure 5 shows examples in which samples with negative values of δ_{v0} (below the RSC) exhibited normal behaviour and Fig. 6 and Fig. 13 show examples in which samples with positive values of δ_{v0} (above the RSC) exhibited reverse behaviour. Moreover, Fig. 14 shows that samples consolidated to states on the RSC exhibit similar behaviours in which changes in confining pressure do not seem to affect their behaviour (neither increase nor decrease their volume change tendencies or normalised liquefaction potential). It may be noticed, therefore, that the occurrence of reverse or normal behaviour depends on the location of the ICL with respect to the RSC for both clean sands and sands with fines. The ICLs that are located below and above the RSC may correspond to the normal and reverse behaviour, respectively. Fig. 14 indicates that RSC itself can be considered as a neutral ICL. This suggests that the RSC might be considered as a special ICL that approximately separates the e–ln p plane into the neutral, normal and reverse behaviour regions.

The change in liquefaction potential of the soils examined can be described readily by applying the new reference curve. Values of δ_{v0} are presented for all samples in Fig. 5, Fig. 6, Fig. 13 and Fig. 14. Examination of these figures reveals that an increase in δ_{v0} is always associated with a less stable behaviour, irrespective of the kind of behaviour

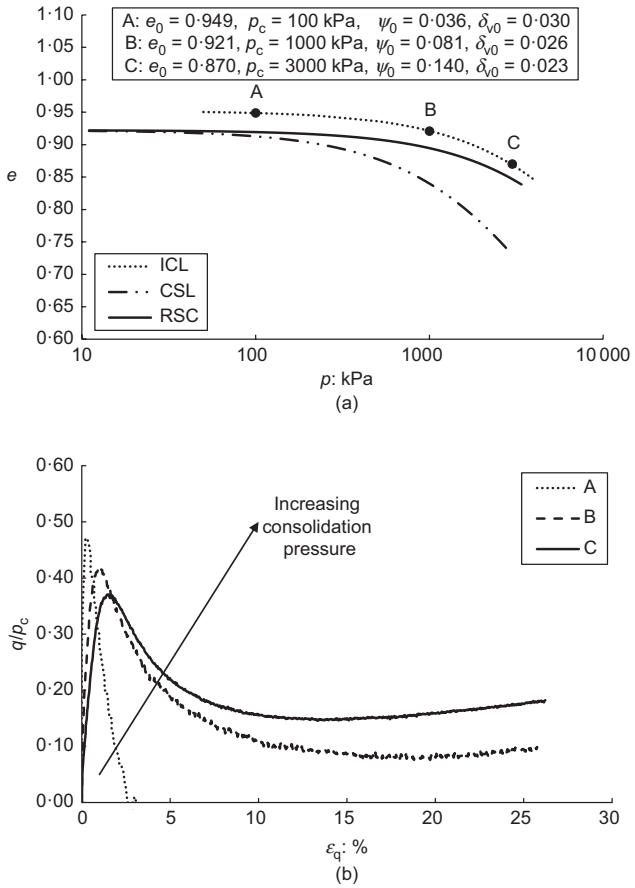

Fig. 13. Effect of consolidation pressure on liquefaction potential of Toyoura sand: (a) initial states; (b) normalised stress–strain responses (test data from Verdugo (1992))

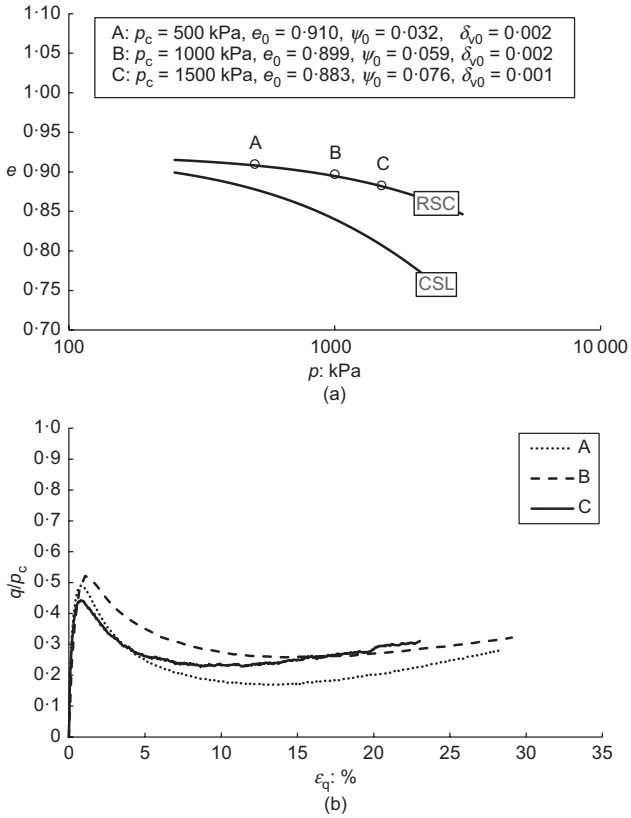

Fig. 14. Effect of consolidation pressure on liquefaction potential of Toyoura sand consolidated to states on the RSC: (a) initial states; (b) normalised stress–strain responses (test data from Verdugo (1992))

(normal, reverse, or neutral) or the kind of material (clean sand or sand mixed with a low percentage of fines). Increase in vertical distance from the initial state to the RSC is therefore associated with increase in liquefaction potential.

SUMMARY AND CONCLUSIONS

State parameters and indices help in understanding and describing the behaviour of soils. They have many applications in geotechnical engineering, where they can be applied either in advanced constitutive models or in simple formulas that can be used by engineers to assess the kind of behaviour that can be expected.

In this paper, the main limitations of the initial state parameter (ψ_0) were described to be: (*a*) the difference in gradation of the soil at the initial and reference states for samples consolidated to high confining pressures; (*b*) poor correlation with M_p over a wide range of confining pressures; and (*c*) inability in describing the reverse behaviour.

A new RSC to define the state index has been presented by taking the effects of particle breakage into account and making the following assumptions: (*a*) the existence of a correlation between the amount of particle breakage and total work input to the specimen; (*b*) stopping of particle breakage at very high stress levels on both CSL and ICLs; (*c*) similarity in breakage index at initial and reference states located on a suitable RSC; (*d*) in the *ln e*–ln *p* plane, the CSL is parallel to the LCC at elevated stress levels; (*e*) changing the gradation of the soil due to particle breakage only imposes a downward shift to the CSL in the *e*–ln *p* plane and does not change its slope significantly.

It was shown that a state index defined using an RSC can be used in the estimation of M_p, describing the reverse behaviour and liquefaction potential of sandy soils. A simple method to approximate the RSC of sands, which is an ICL in nature, was also proposed.

The RSC is an empirical curve that does not represent an asymptotic state. However, using the RSC as the reference line has the following advantages over the CSS.

(*a*) The RSC and its associated state index can be estimated conveniently (using the simplified method), while the determination of the CSS can be very difficult.
(*b*) It can be used for sand with fines and to describe the reverse behaviour; therefore, it might be utilised in the development of unified constitutive models for a wide range of soils.
(*c*) Using the RSC as the reference curve in the calculation of the state index does not require the use of a breakage index. This greatly simplifies its formulation and especially its use in constitutive models.

In conclusion, the use of the new RSC can significantly improve the ability to predict the behaviour of a wide range of soils, including clean sands, sands with fines and clayey soils over a wide range of effective confining stresses and void ratios. It can be used to define new state indices that can be applied to develop unified constitutive models for sandy and clayey soils.

ACKNOWLEDGEMENT

Support from the Spanish ministry of Economy is gratefully acknowledged (Project Geoflow BIAS2012-37020-C02-01 and ALAS BIA2016-76253-P).

NOTATION

A sin ϕ_μ
a parameter used to correlate breakage index to total energy input per unit volume of specimen (MPa)
B_{10} breakage index representing the amount of particle breakage
D_{10f}, D_{10i} effective grain size of the final and initial gradation, respectively. Effective grain size is the maximum particle size of the smallest 10% of the aggregate
E_T total energy input per unit volume of specimen (MPa)
e, e_0, e_{RSC} void ratio, void ratio at the end of consolidation and void ratio at a point on the reference state curve at the initial value of mean effective stress
k_p slope of the variation of $\ln(\sin\phi_p)$ with δ_{v0}
M, M_p stress ratio ($= q/p$) and stress ratio at peak of undrained effective stress path, respectively
N void ratio on the limiting compression curve corresponding to $p = 1$ (unit stress)
p, p_c mean effective stress and its value at the end of consolidation, respectively
p_r, p_{cr}, p'_r parameters to capture the curvature of the isotropic compression curve, the critical state line and reference state curve, respectively
q deviatoric stress
Γ void ratio at the critical state line at $p + p_{cr} = 1$ (unit stress)
Δ horizontal distance of the limiting compression curve and the critical state line at the elevated stress zone in logarithmic scale
δ_{v0} vertical distance from the initial state of a specimen to the reference state curve at the same mean effective stress
$\varepsilon_v, \varepsilon_q, \dot{\varepsilon}_v, \dot{\varepsilon}_q$ volumetric strain, deviatoric strain, volumetric strain increment, deviatoric strain increment
λ slope of the limiting compression curve and critical state line at elevated stress level in ln *e*–ln *p* space
v specific volume
σ_1, σ_3 major and minor principle effective stresses, respectively
ϕ_p mobilised friction angle at peak of undrained effective stress path
ϕ_μ inter-particle friction angle
ψ, ψ_0 vertical distance from the point representing the current and initial states of a specimen to the critical state line at the same mean effective stress, respectively

REFERENCES

Bauer, E. (1996). Calibration of a comprehensive constitutive equation for granular materials. *Soils Found.* **36**, No. 1, 13–26.
Been, K. & Jefferies, M. G. (1985). A state parameter for sands. *Géotechnique* **35**, No. 2, 99–112, http://dx.doi.org/10.1680/geot.1985.35.2.99.
Bobei, D., Lo, S., Wanatowski, D., Gnanendran, C. & Rahman, M. M. (2009). Modified state parameter for characterizing static liquefaction of sand with fines. *Can. Geotech. J.* **46**, No. 3, 281–295.
Bopp, P. A. & Lade, P. V. (2005). Relative density effects on undrained sand behavior at high pressures. *Soils Found.* **45**, No. 1, 15–26.
Butterfield, R. (1979). A natural compression law for soils (an advance on *e*–log *p*′). *Géotechnique* **29**, No. 4, 469–480, http://dx.doi.org/10.1680/geot.1979.29.4.469.
Coop, M. & Lee, I. (1993). *The behaviour of granular soils at elevated stresses.* London, UK: Thomas Telford.
Coop, M., Sorensen, K., Freitas, T. B. & Georgoutsos, G. (2004). Particle breakage during shearing of a carbonate sand. *Géotechnique* **54**, No. 3, 157–164, http://dx.doi.org/10.1680/geot.2004.54.3.157.
De Souza, J. (1958). *Compressibility of sand at high pressure.* Cambridge, MA, USA: Massachusetts Institute of Technology.
Ghafghazi, M., Shuttle, D. & Dejong, J. (2014). Particle breakage and the critical state of sand. *Soils Found.* **54**, No. 3, 451–461.
Hardin, B. O. (1985). Crushing of soil particles. *J. Geotech. Engng* **111**, No. 10, 1177–1192.
Imam, S. M. R., Chan, D. H., Robertson, P. K. & Morgenstern, N. R. (2002a). Effect of anisotropic yielding on the flow liquefaction of loose sand. *Soils Found.* **42**, No. 3, 33–44.

Imam, S. M. R., Morgenstern, N. R., Robertson, P. K. & Chan, D. H. (2002b). Yielding and flow liquefaction of loose sand. *Soils Found.* **42**, No. 3, 19–31.

Imam, S. M. R., Morgenstern, N. R., Robertson, P. K. & Chan, D. H. (2005). A critical-state constitutive model for liquefiable sand. *Can. Geotech. J.* **42**, No. 3, 830–855.

Ishihara, K. (1993). Liquefaction and flow failure during earthquakes. *Géotechnique* **43**, No. 3, 351–451, http://dx.doi.org/10.1680/geot.1993.43.3.351.

Ishihara, K., Cubrinovski, M. & Nonaka, T. (1998). Characterization of undrained behaviour of soils in the reclaimed area of Kobe. *Soils Found.* **38**, Special Issue, 33–46.

Ladd, C. C. & Foott, R. (1974). New design procedure for stability of soft clays: 10F, 3T, 39R. *J. Geotech. Engng. Div.* **100**, No. GT7, 763–786.

Lade, P. V. (1992). Static instability and liquefaction of loose fine sandy slopes. *J. Geotech. Engng* **118**, No. 1, 51–71.

Lade, P. V. & Yamamuro, J. A. (1997). Effects of nonplastic fines on static liquefaction of sands. *Can. Geotech. J.* **34**, No. 6, 918–928.

Lade, P. V., Yamamuro, J. A. & Bopp, P. A. (1996). Significance of particle crushing in granular materials. *J. Geotech. Engng* **122**, No. 4, 309–316.

Li, X. & Dafalias, Y. F. (2000). Dilatancy for cohesionless soils. *Géotechnique* **50**, No. 4, 449–460, http://dx.doi.org/10.1680/geot.2000.50.4.449.

Manzari, M. T. & Dafalias, Y. F. (1997). A critical state two-surface plasticity model for sands. *Géotechnique* **47**, No. 2, 255–272, http://dx.doi.org/10.1680/geot.1997.47.2.255.

Marsal, R. J. (1967). Large-scale testing of rockfill materials. *J. Soil Mech. Found. Div.* **93**, No. 2, 27–43.

McDowell, G., Bolton, M. & Robertson, D. (1996). The fractal crushing of granular materials. *J. Mech. Phys. Solids* **44**, No. 12, 2079–2101.

Miura, N. & O-Hara, S. (1979). Particle-crushing of a decomposed granite soil under shear stresses. *Soils Found.* **19**, No. 3, 1–14.

Miura, N., Murata, H. & Yasufuku, N. (1984). Stress–strain characteristics of sand in a particle-crushing region. *Soils Found.* **24**, No. 1, 77–89.

Muir Wood, D. (1990). *Soil behaviour and critical state soil mechanics*. Cambridge, UK: Cambridge University Press.

Muir Wood, D. (2007). The magic of sands. *Can. Geotech. J.* **44**, No. 11, 1329–1350.

Muir Wood, D. & Maeda, K. (2008). Changing grading of soil: effect on critical states. *Acta Geotechnica* **3**, No. 1, 3–14.

Muir Wood, D., Belkheir, K. & Liu, D. (1994). Strain softening and state parameter for sand modelling. *Géotechnique* **44**, No. 2, 335–339, http://dx.doi.org/10.1680/geot.1994.44.2.335.

Pestana, J. (1994). *A unified constitutive model for sands and clays*. ScD thesis, Department of Civil Engineering, Massachusetts Institute of Technology, Cambridge, MA, USA.

Pestana, J. M. & Whittle, A. (1995). Compression model for cohesionless soils. *Géotechnique* **45**, No. 4, 611–632, http://dx.doi.org/10.1680/geot.1995.45.4.611.

Pestana, J. M. & Whittle, A. J. (1999). Formulation of a unified constitutive model for clays and sands. *Int. J. Numer. Analyt. Methods Geomech.* **23**, No. 12, 1215–1243.

Rahman, M. M. & Lo, S. (2014). Undrained behavior of sand-fines mixtures and their state parameter. *J. Geotech. Geoenviron. Engng* **140**, No. 7, 04014036.

Roscoe, K. & Burland, J. B. (1968). On the generalized stress–strain behaviour of wet clay. In *Engineering Plasticity* (eds J. Heyman and F. A. Leckie), pp. 535–609. Cambridge, UK: Cambridge University Press.

Russell, A. R. & Khalili, N. (2004). A bounding surface plasticity model for sands exhibiting particle crushing. *Can. Geotech. J.* **41**, No. 6, 1179–1192.

Sheng, D., Yao, Y. & Carter, J. P. (2008). A volume–stress model for sands under isotropic and critical stress states. *Can. Geotech. J.* **45**, No. 11, 1639–1645.

Sladen, J., D'Hollander, R. & Krahn, J. (1985). The liquefaction of sands, a collapse surface approach. *Can. Geotech. J.* **22**, No. 4, 564–578.

Taiebat, M. & Dafalias, Y. F. (2008). SANISAND: simple anisotropic sand plasticity model. *Int. J. Numer. Analyt. Methods Geomech.* **32**, No. 8, 915–948.

Vaid, Y. P. & Chern, J. C. (1985). Cyclic and monotonic undrained response of saturated sands. In *Advances in the art of testing soils under cyclic conditions* (ed. V. Khosla), pp. 120–147. New York, NY, USA: American Society of Civil Engineers (ASCE).

Verdugo, R. (1992). *Characterization of sandy soil behavior under large deformation*. Tokyo, Japan: University of Tokyo.

Vesic, A. S. & Clough, G. W. (1968). Behavior of granular materials under high stresses. *J. Soil Mech. Found. Div* **94**, No. SM3, 661–688.

Vilhar, G., Jovičić, V. & Coop, M. R. (2013). The role of particle breakage in the mechanics of a non-plastic silty sand. *Soils Found.* **53**, No. 1, 91–104.

Wan, R. & Guo, P. (1998). A simple constitutive model for granular soils: modified stress–dilatancy approach. *Comput. Geotech.* **22**, No. 2, 109–133.

Wang, Z. L., Dafalias, Y. F., Li, X. S. & Makdisi, F. I. (2002). State pressure index for modeling sand behavior. *J. Geotech. Geoenviron. Engng* **128**, No. 6, 511–519.

Yamamuro, J. A. & Lade, P. V. (1998). Steady-state concepts and static liquefaction of silty sands. *J. Geotech. Geoenviron. Engng* **124**, No. 9, 868–877.

Yoshimine, M. (1996). *Undrained flow deformation of saturated sand under monotonic loading conditions*. Doctor of Engineering thesis, University of Tokyo, Tokyo, Japan.